Aerosol Science and Technology

ISSN: 0278-6826 (Print) 1521-7388 (Online) Journal homepage: http://www.tandfonline.com/loi/uast20

The Effects of Monomer Size Distribution on the Radiative Properties of Black Carbon Aggregates

Chao Liu, Yan Yin, Fangchao Hu, Hongchun Jin & Christopher M. Sorensen

To cite this article: Chao Liu, Yan Yin, Fangchao Hu, Hongchun Jin & Christopher M. Sorensen (2015) The Effects of Monomer Size Distribution on the Radiative Properties of Black Carbon Aggregates, Aerosol Science and Technology, 49:10, 928-940, DOI: 10.1080/02786826.2015.1085953

To link to this article: http://dx.doi.org/10.1080/02786826.2015.1085953

Accepted online: 26 Aug 2015.

Aerosol Science and Technology, 49:928–940, 2015

ISSN: 0278-6826 print / 1521-7388 online
DOI: 10.1080/02786826.2015.1085953

The Effects of Monomer Size Distribution on the Radiative Properties of Black Carbon Aggregates

Chao Liu,[1] Yan Yin,[1,2] Fangchao Hu,[1] Hongchun Jin,[3] and Christopher M. Sorensen[4]

[1]*Key Laboratory for Aerosol-Cloud-Precipitation of China Meteorological Administration, School of Atmospheric Physics, Nanjing University of Information Science and Technology, Nanjing, China*
[2]*Collaborative Innovation Center on Forecast and Evaluation of Meteorological Disasters, Nanjing University of Information Science and Technology, Nanjing, China*
[3]*Key Laboratory for Semi-Arid Climate Change of the Ministry of Education, Lanzhou University, Lanzhou, China*
[4]*Department of Physics, Kansas State University, Manhattan, Kansas, USA*

Black carbon (BC), normally existing as aggregates, significantly affects the Earth radiative forcing, energy balance, and climate by scattering and absorbing both solar radiation and terrestrial emission. The BC particles are usually treated as fractal aggregates with same-sized monomers. However, experimental studies show that monomer diameters of BC normally obey a lognormal distribution ranging from 10 nm to over 100 nm. This study investigates the effects of monomer size distribution on the radiative properties of BC particles. The fractal aggregates are generated by a cluster–cluster aggregation (CCA) algorithm, and the Multiple Sphere T-Matrix (MSTM) method is used to simulate the radiative properties of randomly oriented aggregates. The integral radiative properties of aggregates with different-sized monomers have normal distributions with large standard deviations, and it requires to average radiative properties of over 60 aggregate realizations to represent their ensemble-averaged properties. The aggregates with different-sized monomers exhibit much stronger scattering and absorption than the aggregates with same-sized monomers and the geometric mean diameter, whereas the absorption cross section becomes comparable to that given by aggregates with same-sized monomer and the equivalent volume diameter. Similar phase matrix elements are obtained for the aggregates with different-sized and same-sized monomers. Furthermore, the Rayleigh-Debye-Gans (RDG) approach is significantly challenged for approximating the absorption and scattering cross sections of the aggregates with different-sized monomers, whereas it performs quite accurately for the phase matrix elements.

Received 18 May 2015; accepted 31 July 2015.
Address correspondence to Chao Liu, Key Laboratory for Aerosol-Cloud-Precipitation of China Meteorological Administration, School of Atmospheric Physics, Nanjing University of Information Science and Technology, Nanjing 210044, China. E-mail: chao_liu@nuist.edu.cn
Color versions of one or more figures in this article can be found online at www.tandfonline.com/lmsa.

1. INTRODUCTION

Black carbon (BC), also known as soot, is an important aerosol in the atmosphere, especially in urban regions. BC plays a significant role in the Earth's radiation budget by absorbing and scattering both solar and terrestrial radiation (Alexander et al. 2008; Moffet and Prather 2009). As the major absorber of visible solar radiation, BC can heat the air, alter regional atmospheric stability, and, thus, affect the large-scale circulation and hydrological cycle with significant climate effects (Menon et al. 2002; Ramanathan and Carmichael 2008). However, large uncertainties in estimating soot direct and indirect effects still exist due to the lack of understanding on the associated radiative properties. Accurate parameterization of the radiative properties becomes fundamental to fully account for their effects on radiative forcing, climate, and feedback.

Laboratorial measurements, based on the Scanning Electron Microscopy (SEM) and Transmission Electron Microscopy (TEM), confirm that soot particles are normally in the form of cluster-like aggregates with numerous spherical primary particles (Cai et al. 1993; Dobbins et al. 1998; Tian et al. 2004; Helas et al. 2006; Dukhin et al. 2007). The overall soot aggregate morphology can be well described by fractal geometries, i.e., fractal aggregates. The fractal aggregates obey the statistical scaling law in the form of (Forrest and Witten 1979; Sorensen and Roberts 1997; Sorensen 2001):

$$N = k_f \left(\frac{2R_g}{d_{\text{mon}}} \right)^{D_f} \quad [1]$$

Here, N, the number of primary particles (monomers) in an aggregate, represents the overall aggregate size, and d_{mon} is the diameter of those "same-sized" monomers. The fractal dimension D_f and fractal prefactor k_f are the parameters

determining structures of BC aggregates. In Equation (1), R_g is known as the gyration radius that infers the overall aggregate size in length scale, and is given by $R_g^2 = \frac{1}{N}\sum_{i=1}^{N}(\vec{r_i} - \vec{r_o})^2$. Here, $\vec{r_o}$ is the position vector of the cluster's mass center, and $\vec{r_i}$ indicates the position vector of the *i*th monomer's center.

The monomers, i.e., primary particles, are always assumed as same-sized homogeneous spheres, and are known as a minor factor to determine BC radiative properties besides the overall aggregate structure. For simplification, numerical studies on BC clusters always assume the monomers to have exactly the same diameter and to attach with others without overlapping. However, some experimental studies indicate that this is not true for realistic BC aggregates: the monomer diameters were found to vary from approximately 10 nm to over 100 nm following a lognormal size distribution (Köylü and Faeth 1992, 1994; Lehre et al. 2003; Dankers and Leipertz 2004; Chakrabarty et al. 2006, 2007; Liu et al. 2006; Bescond et al. 2014). Bescond et al. (2014) presented an automated method for determination of the monomer size distribution, and also show the wide variation on monomer diameters. All those studies show a lognormal size distribution for the monomers in the form of:

$$p(d_{\mathrm{mon}}) = \frac{dN}{dd_{\mathrm{mon}}} = \frac{1}{d_{\mathrm{mon}}\sqrt{2\pi}\ln\sigma} exp\left[-\left(\frac{\ln(d_{\mathrm{mon}}/d_{\mathrm{geo}})}{\sqrt{2}ln\sigma}\right)^2\right] \quad [2]$$

Here, d_{geo} is the geometric mean of monomer diameters, and the geometric standard deviation σ exhibits values from 1.1 to over 1.6 from various observations (Köylü and Faeth 1992, 1994; Lehre et al. 2003; Dankers and Leipertz 2004; Chakrabarty et al. 2006, 2007; Liu et al. 2006; Bescond et al. 2014). It should be noticed that the size distribution in Equation (2) is normalized. The monomer size distribution is usually neglected as a minor factor besides the overall aggregate structure and size, whereas some studies do notice the importance of polydispersity of monomer diameter on the radiative properties of BC aggregates (Farias et al. 1996a; Charalampopoulos and Shu 2002; Yin and Liu 2010). Farias et al. (1996a) show that the monomer size distribution has a significant effect on the aggregate absorption, and a recent study by Yin and Liu (2010) calculates the radiative properties of aggregates with four monomer diameters. To have a more accurate knowledge on the radiative properties of BC clusters, this study quantitatively and systematically investigates the effects of monomer size distribution on the radiative properties of BC aggregates.

A number of numerical models, both approximated and exact ones, have been developed and applied to calculate the radiative properties of fractal aggregates. The Rayleigh-Debye-Gans (RDG) method is one of the simplest and most popular approximations. The RDG is a highly efficient method to approximate the scattering and absorption by aggregates with small monomers, whereas sometimes yields relative errors even larger than 15% (Sorensen et al. 1992; Cai et al. 1993; Farias et al. 1996b; Sorensen 2001; Van-Hulle et al. 2002; Berg and Sorensen 2013). Numerically exact methods, such as the Multiple Sphere T-Matrix method (MSTM) (also known as the Superposition T-matrix method; Mackowski 1994; Mackowski and Mishchenko 1996; Liu and Mishchenko 2005, 2007) and the Generalized Multi-particle Mie (GMM) method (Xu 1995; Xu and Gustafson 2001; Li et al. 2010; Liu and Smallwood 2010b, 2011; Liu et al. 2013), are also widely used to simulate the radiative properties of soot aggregates. Different from the RDG, both the MSTM and GMM are used to calculate light scattering by each aggregate realization, and require the exact configuration of an aggregate, i.e., the position and size of each monomer. We choose the MSTM method to give the exact radiative properties of randomly oriented aggregates, and will discuss results on the extinction, scattering, and absorption cross sections (C_{ext}, C_{sca} and C_{abs}), single-scattering albedo (*SSA*), asymmetry factor (g), and phase matrix of BC aggregates (van de Hulst 1957). One of MSTM's advantages is that it calculates the radiative properties of randomly oriented aggregates analytically and efficiently, and it is not necessary to obtain the results by averaging those over different particle orientations. However, the applicability of both the GMM and MSTM is limited to aggregates of spheres without overlapping. Methods such as the finite-difference time domain method (Yee 1966; Yang and Liou 1996), pseudo-spectral time domain method (Liu 1997; Liu et al. 2012a), and discrete dipole approximation (Purcell and Pennypacker 1973; Yurkin and Hoekstra 2011) are more flexible on particle geometries, and have been used for aggregates with overlapping monomers (Skorupski and Mroczka 2014; Yon et al. 2015).

This study investigates the radiative properties of aggregates with different-sized monomers. The numerical algorithm to generate the aggregates will be detailed in Section 2. Section 3 shows the results on the ensemble-averaged radiative properties of aggregates with different-sized and same-sized monomers, and discusses the modified RDG approaches for aggregates with different-sized monomers. Section 4 concludes this work.

2. AGGREGATES WITH DIFFERENT-SIZED MONOMERS

Since its introduction in 1970s, the concept of "fractal aggregate" has been widely used to represent BC particles, and both theoretical and experimental efforts were extensively conducted on the principle and parameterization of the fractal aggregates and their properties. The radiative

properties of soot aggregates with same-sized monomers have been reviewed by Martin and Hurd (1987), Charalampopoulos (1992), and Sorensen (2001). The community seems to accept and be satisfied to use the aggregates with same-sized monomers, whereas observations have shown a clear and wide size distribution for soot monomers (Köylü and Faeth 1992, 1994; Lehre et al. 2003; Chakrabarty et al. 2006, 2007; Liu et al. 2006; Bescond et al. 2014). As we know, the statistic scaling rule and the definition of R_g given above are strictly valid for aggregates with same-sized monomers, whereas our knowledge on the structures of aggregates with different-sized monomers is still quite limited (Farias et al. 1996a; Eggersdorfer and Pratsinis 2012). However, this study focuses on the radiative properties of aggregates with different-sized monomers, and we discuss our results by comparing with those of aggregates with same-sized monomers. Thus, to make the comparison fair and meaningful, it would be best and reasonable to keep using the same aggregate concepts and parameters as those with same-sized monomers. Furthermore, the structure of aggregates consisting polydisperse monomers was studied by Eggersdorfer and Pratsinis (2012), and their results indicated that the effects of monomer polydispersity on the fractal dimension and prefactor are relatively weak when the geometric standard deviation is less than 1.5 (maximum value used in this study). As a result, we will modify the configurations of the soot aggregates only by introducing different-sized monomers, and assume that the aggregates with the different-sized monomers still follow

$$N = k_f \left(\frac{2R_g}{d_{\text{geo}}} \right)^{D_f}, \qquad [3]$$

i.e., the statistic scaling rule of aggregates with same-sized monomers having the geometric mean diameter. With different-sized monomers, the expression for the gyration radius should also be modified as the following (Eggersdorfer and Pratsinis 2012):

$$R_g^2 = \frac{\sum_{i=1}^{N} m_i (\vec{r_i} - \vec{r_o})^2}{\sum_{i=1}^{N} m_i} \qquad [4]$$

To keep aggregate structures of the two kinds similar and comparable, a tunable cluster–cluster aggregation (CCA) algorithm, developed by Filippov et al. (2000), is modified to generate fractal aggregates with given fractal parameters but different-sized monomers. The procedure of particle aggregation, which can be found in Filippov et al. (2000) and Liu et al. (2012b), is not changed, and, thus, we will not give the details here. This study considers a lognormal size distribution for the monomers, in the form of Equation (2), which is found to provide an accurate agreement to measurements. Thus, the only difference from the original CCA is that the monomer diameters are determined randomly and follow the given size distribution. Before performing the aggregation algorithm, we first determine the diameter of each monomer by a random number, and the resulting diameters follow the lognormal distribution with given d_{geo} and σ. N monomers with determined but different diameters would then form aggregates following the CCA until a final cluster is generated. Because we assume that aggregates with different-sized monomers still follow the statistic scaling rule of aggregates with same-sized ones having the geometric mean diameter, fixed value of d_{geo} is used to determine the relative distance of two aggregates added together during the CCA.

Each aggregate generated with specified monomer sizes and aggregate structure is referred as an aggregate realization. Figure 1 gives some examples of aggregates containing different-sized monomers, and the five aggregates have the monomer numbers of $N = 50$, 100, 200, 300, and 500. The geometric mean diameter and geometric standard deviation are 33 nm and 1.275, respectively, and the monomer size differences can be seen clearly form the figure. The fractal parameters of $D_f = 1.82$ and $k_f = 1.19$, which are typical values for BC particles, are used for the figure (Sorensen and Roberts 1997; Sorensen 2001).

The aggregates with different-sized monomers are generated based on the lognormal size distribution and the CCA algorithm, and the MSTM method is used to calculate their exact scattering and absorption properties. This study fixes the fractal parameters as $D_f = 1.82$ and $k_f = 1.19$, suggested by Sorensen and Roberts (1997). Two sets of monomer size distributions, both of which are based on observations, will be discussed: (1) $d_{\text{geo}} = 33$ nm and $\sigma = 1.275$ given by Liu et al. (2006); and, (2) $d_{\text{geo}} = 45.5$ nm and $\sigma = 1.13$ measured by Chakrabarty et al. (2007). Values similar to $d_{\text{geo}} = 33$ nm and $\sigma = 1.275$ were also obtained by Bescond et al. (2014), and Chakrabarty et al. (2006) show standard deviations as large as 1.6. The incident wavelength is chosen to be 650 nm, and the corresponding BC refractive index of 1.75 + 0.435i is used (d'Almeida et al. 1991; Liu and Mishchenko 2007; Li et al. 2010, 2012b). To demonstrate the importance of monomer size distribution, the radiative properties of aggregates with different-sized monomers will be compared with those based on same-sized monomers. Of course, the comparison is carried out for aggregates with the same N, and two diameter cases for the aggregates with same-sized monomers will be considered. One uses the geometric mean diameter, i.e., d_{geo} of Equation (2). The other diameter is used to make the aggregate with same-sized monomers to have the same volume as that of the aggregate with different-sized monomers, and it will be referred as the "equivalent volume" diameter, i.e., d_{vol}. Mathematically, the "equivalent-volume" diameter

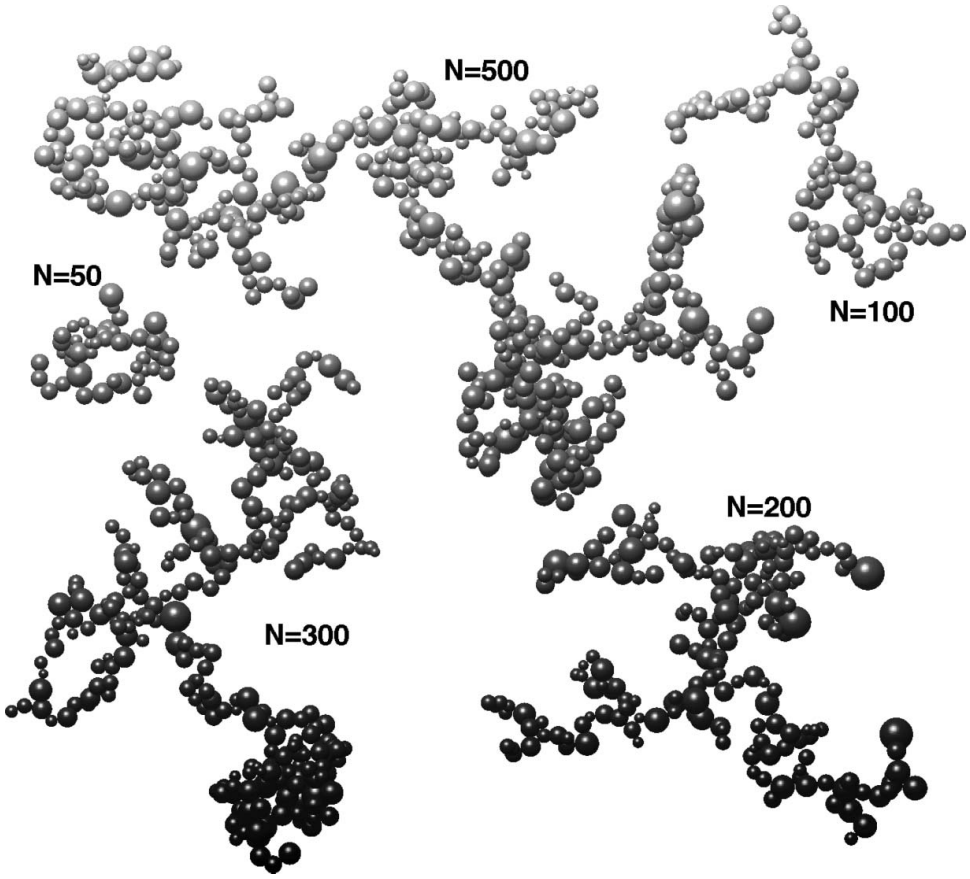

FIG. 1. Examples of fractal aggregates with different-sized monomers, numerically generated using a cluster–cluster aggregation algorithm with N = 50, 100, 200, 300, and 500. The fractal parameters of the aggregates are $D_f = 1.82$ and $k_f = 1.19$, and the monomers follow the lognormal distribution with $d_{geo} = 33$ nm and $\sigma = 1.275$.

satisfies:

$$N\frac{\pi d_{vol}^3}{6} = N\int \frac{\pi d_{mon}^3}{6} p(d_{mon}) dd_{mon} = N\frac{\pi d_{geo}^3}{6} exp(4.5\ln^2\sigma) \quad [5]$$

Then, we obtain the relationship between the two diameters as $d_{vol} = d_{geo}\sqrt[3]{\exp(4.5\ln^2\sigma)}$. The first term of Equation (5) is the total volume of the aggregate with N same-sized monomers, each of which has a diameter of d_{vol}, and the term in the middle is that of the aggregate with monomer size distribution given by Equation (2).

For atmospheric applications, what are really meaningful are the ensemble-averaged radiative properties of particles. The randomly generated aggregates in this study will have not only different overall aggregate structures but also different monomer sizes, and different aggregate realizations are expected to show even more significant variations on their radiative properties. Thus, this study focuses on the radiative properties averaged over different aggregate realizations with the given aggregate parameters (N, D_f, and k_f) and monomer parameters (d_{geo} and σ).

3. RESULTS AND DISCUSSION

The radiative properties of aggregates with 200 different-sized monomers (i.e., $N = 200$) are studied as an example. To generate the aggregates, the sizes of monomers in each aggregate are randomly generated with the pseudo-random number generator, and an example of monomer diameter distribution, as well as the lognormal probability distribution function, is shown in the left panel of Figure 2. We generate 500 different aggregate realizations using the CCA, and nine examples of aggregate realizations with different-sized monomers are shown in the right side of Figure 2. The geometric mean diameter and the geometric standard deviation are 33 nm and 1.275, respectively. The numerically generated monomer sizes follow the theoretical distribution really well. The aggregates clearly show the variations on both overall aggregation geometries and monomer diameters, and we will discuss how

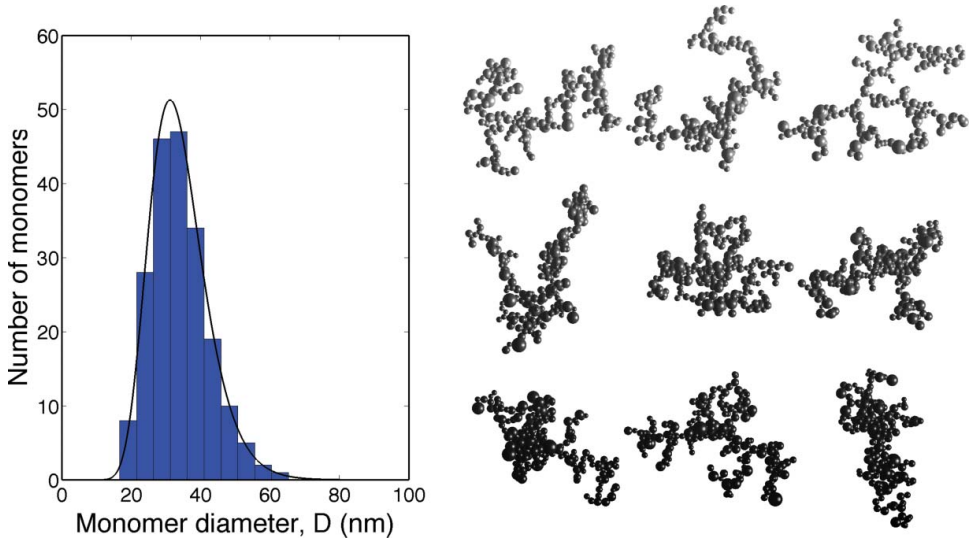

FIG. 2. Monomer size realizations generated following the lognormal distribution (left) and nine examples of aggregates with different configurations but same monomer size realization. The lognormal probability distribution function has a geometric mean of 33 nm and the geometric standard deviation of 1.275.

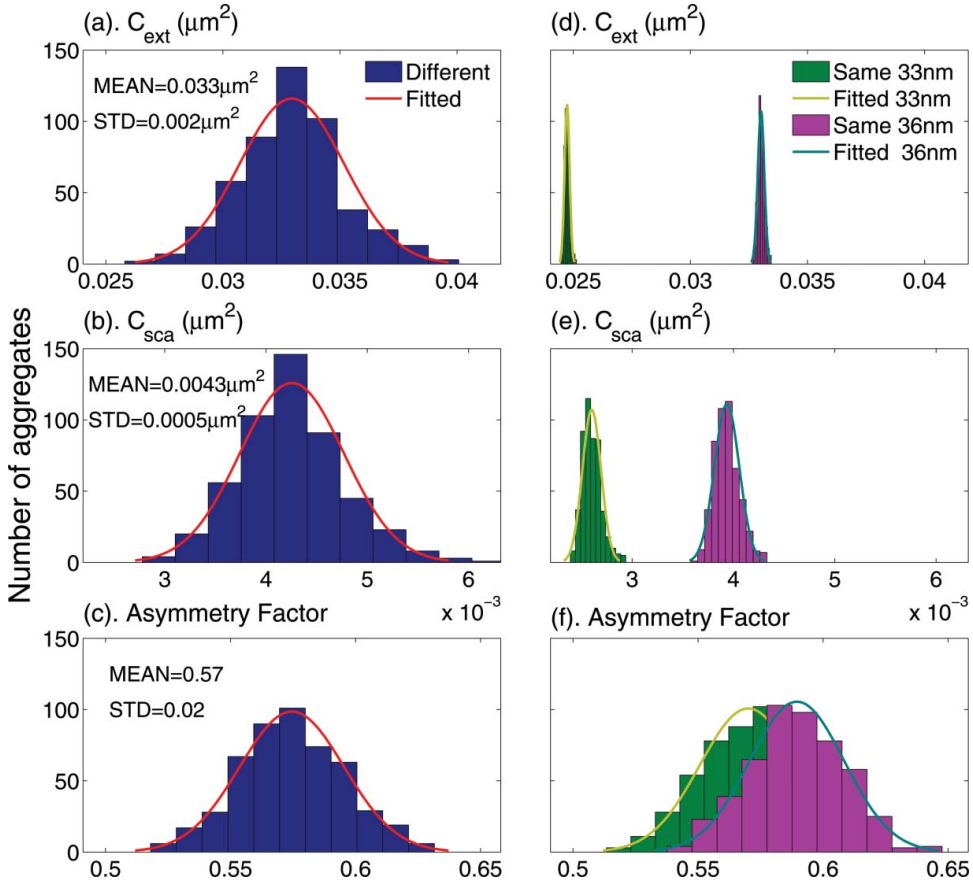

FIG. 3. Distributions of the extinction cross sections, scattering cross sections, and asymmetry factors for aggregates with different-sized (left) and same-sized (right) monomers, and the fitted normal distribution functions are also given in the figure. Five hundred different realizations are used for each case, and the diameters of 33 nm and 36 nm are used for aggregates with same-sized monomers.

significantly these differences may influence their radiative properties.

Figure 3 shows the number distributions of the integral scattering properties for 500 aggregates with different-sized (left panels) and same-sized (right panels) monomers, and the fitted normal probability distribution functions based on their mean values and standard deviations are also illustrated in the figure. The same monomer size distribution as that for Figure 2 is used for aggregates with different-sized monomers. Meanwhile, $d_{geo} = 33$ nm and $d_{vol} = d_{geo}\sqrt[3]{\exp(4.5\ln^2\sigma)} = 36$ nm are used for the two cases of aggregates with same-sized monomers. The left column is for the properties of aggregates with different-sized monomers, and the right one is for the two cases with same-sized monomers. The mean values (as "MEAN" in the figure) and standard deviations (as "STD" in the figure) of the corresponding quantities of aggregates with different-sized monomers are listed in the figure. The extinction cross sections (top panels), scattering cross sections (middle panels), and asymmetry factor (bottom panels) all show excellent agreements with the normal distributions. However, the differences between the radiative properties of aggregates with different-sized and same-sized monomers can be clearly seen in the figure. First, the cross sections of the aggregates with different-sized monomers vary in much wider ranges than those of the same-sized ones (i.e., much larger standard deviations), and this is because of different monomer sizes in different aggregate realizations. Second, when compared with the aggregates with same-sized monomers of $d_{geo} = 33$ nm, the aggregates with different-sized monomers show much larger extinction and scattering cross sections (the mean values are 32% and 65% larger, respectively). If the diameter of same-sized monomers increases to $d_{vol} = 36$ nm, the extinction cross sections for aggregates with different-sized and same-sized monomers have similar mean values, whereas the mean scattering cross section of the same-sized ones is still approximately 10% smaller than that of the different-sized ones. Third, the asymmetry factors of aggregates with different-sized and same-sized monomers show both similar distributions and mean values. The mean value increases a little bit (4%) as the diameter increases for aggregates with same-sized monomers (from $d_{geo} = 33$ nm to $d_{vol} = 36$ nm). The results of the absorption cross sections are similar to those of the extinction cross sections (as the extinction is dominated by the absorption, approximately 87%), and are not given in the figure. Figure 3 indicates that the monomer size distribution can significantly influence the cross sections of the aggregates, whereas it has little effect on the asymmetry factors.

Table 1 lists the mean values and the ratios of standard deviations to mean values of the radiative properties of aggregates given by the MSTM. The parameters for the aggregates with different-sized and same-sized monomers are the same as those used for Figure 3, and some of the data has been listed and discussed above. Again, it is obvious that the aggregates with different-sized and same-sized monomers (with $d_{geo} = 33$ nm) have quite different cross sections, and the relative differences on the scattering and absorption cross sections can be as large as 40% and 25%, respectively. If aggregate with same-sized monomers use $d_{vol} = 36$ nm, it only underestimates the scattering by 10%. However, not only the mean values of the asymmetry factors, i.e., g in the table, but also their standard deviations are almost the same for aggregates with different-sized and same-sized monomers (both d_{geo} and d_{vol}), and this has also been illustrated in Figure 3. The second case ($d_{geo} = 45.5$ nm and $\sigma = 1.13$) has smaller standard deviation, and similar results are obtained.

As one of the most popular and efficient approaches, the RDG approximation has been widely used to calculate the

TABLE 1
Comparison between the ensemble-averaged integral radiative properties of aggregates with different-sized and same-sized monomers given by the MSTM

Ensemble-averaged integral radiative properties		C_{ext} Mean (μm^2)	C_{ext} Ratio[a] (%)	C_{sca} Mean (μm^2)	C_{sca} Ratio (%)	C_{abs} Mean (μm^2)	C_{abs} Ratio (%)	g Mean	g Ratio (%)
Aggregates with different-sized monomers (d_{geo} = 33 nm and σ = 1.275)		0.033	6.7	0.0043	12	0.029	6.0	0.57	3.6
Aggregates with same-sized monomers	d_{geo} = 33 nm	0.025	0.43	0.0026	3.5	0.022	0.18	0.57	3.4
	d_{vol} = 36 nm	0.033	0.42	0.0039	3.1	0.029	0.19	0.59	3.2
Aggregates with different-sized monomers (d_{geo} = 45.5 nm and σ = 1.13)		0.076	3.1	0.013	5.7	0.063	2.6	0.63	2.6
Aggregates with same-sized monomers	d_{geo} = 45.5 nm	0.070	0.50	0.011	3.1	0.059	0.19	0.63	2.5
	d_{vol} = 46.5 nm	0.075	0.49	0.012	3.0	0.063	0.18	0.63	2.5

[a]Ratio in this table refers to the ratio of the standard deviations to the mean values.
Both mean values and the ratios of their standard deviations to the mean values are listed in the table. The optical properties of 500 aggregates are averaged for each case.

radiative properties of aggregates with same-sized monomers (Sorensen 2001), although its accuracy is significantly challenged. This study also investigates the RDG performance on aggregates with different-sized monomers. The RDG algorithm approximates the total scattering and absorption cross sections of aggregates with same-sized monomers by

$$C_{\text{sca, RDG}} = N^2 C_{\text{sca, mon}}\, g(kR_g, D_f), \quad [6]$$

$$C_{\text{abs, RDG}} = N C_{\text{abs, mon}}, \quad [7]$$

where k is the wavenumber, and $g(kR_g, D_f)$ is the scattering factor of the aggregate (Sorensen 2001). $C_{\text{sca, RDG}}$ and $C_{\text{abs, RDG}}$ represent the scattering and absorption cross sections of the aggregate, respectively, and $C_{\text{abs, mon}}$ and $C_{\text{abs, mon}}$ are the corresponding values for the monomer, which are given by the Rayleigh approximation following $C_{\text{sca, mon}} = \frac{\pi}{24} k^4 {d_{\text{mon}}}^6 F(m)$ and $C_{\text{abs, mon}} = \frac{\pi}{2} k {d_{\text{mon}}}^3 F(m)$. Here, d_{mon}, monomer diameter, is a constant for aggregates with same-sized monomers. $E(m)$ and $F(m)$ are functions of particle complex refractive index m. The cross sections of different-sized monomers are different, and the RDG algorithm has to be modified. We present two kinds of simple adjustments that can be made to approximate "effective" $C_{\text{sca, mon}}$ and $C_{\text{abs, mon}}$ of different-sized monomers.

The first approach is to replace the cross sections of same-sized monomers in Equations (6) and (7) using corresponding average values of different-sized monomers. The averaged scattering and absorption cross sections of lognormal-distributed monomers are given by

$$\begin{aligned}\overline{C}_{\text{sca, mon}} &= \int C_{\text{sca, mon}}(d_{\text{mon}}) p(d_{\text{mon}}) d d_{\text{mon}} \\ &= \frac{\pi}{24} k^4 {d_{\text{geo}}}^6 \exp(18\ln^2\sigma) F(m),\end{aligned} \quad [8]$$

$$\begin{aligned}\overline{C}_{\text{abs, mon}} &= \int C_{\text{abs, mon}}(d_{\text{mon}}) p(d_{\text{mon}}) d d_{\text{mon}} \\ &= \frac{\pi}{2} k {d_{\text{geo}}}^3 \exp(4.5\ln^2\sigma) E(m).\end{aligned} \quad [9]$$

Again, the Rayleigh approximation is used for cross sections of each monomer. Thus, the cross sections of the first adjustment, i.e., "RDG 1," for aggregates with different-sized monomers are given by

$$\begin{aligned}C_{\text{sca, RDG1}} &= N^2 \overline{C}_{\text{sca,mon}} g(kR_g, D_f) \\ &= N^2 \frac{\pi}{24} k^4 {d_{\text{geo}}}^6 \exp(18\ln^2\sigma) F(m) g(kR_g, D_f),\end{aligned} \quad [10]$$

$$C_{\text{abs,RDG1}} = N \overline{C}_{\text{abs,mon}} = N \frac{\pi}{2} k {d_{\text{geo}}}^3 \exp(4.5\ln^2\sigma) E(m). \quad [11]$$

The second approach is more straightforward by directly using an effective diameter d_{eff}, i.e., replacing the different-sized monomers by effective ones with the same diameter d_{eff}. We use the equivalent volume diameter d_{vol} as the effective diameter d_{eff}, and get the expressions for the second adjustment, i.e., "RDG 2," as the following:

$$\begin{aligned}C_{\text{sca,RDG2}} &= N^2 C_{\text{sca,mon}}(d_{\text{eff}}) g(kR_g, D_f) \\ &= N^2 \frac{\pi}{24} k^4 {d_{\text{geo}}}^6 \left[\exp(4.5\ln^2\sigma)\right]^2 F(m) g(kR_g, D_f),\end{aligned} \quad [12]$$

$$C_{\text{abs, RDG2}} = N C_{\text{abs,mon}}(d_{\text{eff}}) = \frac{\pi}{2} k {d_{\text{geo}}}^3 \exp(4.5\ln^2\sigma) E(m). \quad [13]$$

This approach is similar to that used by Farias et al. (1996a) besides different monomer size distributions considered. Because the "equivalent volume" diameter is used for the RDG 2, the two RDG approaches yield the same absorption cross section.

Both the absorption under the Rayleigh approximation and volume of a single monomer are proportional to the third power of the monomer diameter, whereas the scattering is proportional to the sixth power. This is the reason that the absorption cross sections of aggregates with different-sized monomers are close to those with same-sized monomers of "equivalent volume" diameter d_{vol}. We assumed the statistic scaling rule and the gyration radius of the aggregates with different-sized monomers follow those of aggregates with same-sized monomer and the geometric diameter, so both the RDG 1 and RDG 2 use the same constant gyration radius given by the geometric mean diameter, i.e., $R_g = \frac{d_{\text{geo}}}{2} \left(\frac{N}{k_f}\right)^{\frac{1}{D_f}}$. Without change for the gyration radius, the RDG approximation for the normalized phase matrix elements is not changed for aggregates with different-sized monomers, and we will not give the details here. The comparison on the angular-dependent properties given by the MSTM and RDG will be discussed later. Considering that a large number of monomers are required to satisfy the lognormal size distribution, the RDG results are understood as those of an ensemble of properties for any aggregate size.

Table 2 compares the integral scattering properties of aggregates with different-sized monomers given by the numerically exact MSTM method and the two RDG approximations. Again, aggregates with 200 monomers are considered, and the geometric parameters (k_f, D_f, d_{geo}, and σ) are the same as those used for Figure 3 and Table 1. For the first case with $d_{\text{geo}} = 33$ nm and $\sigma = 1.275$, the RDG 1 underestimates the absorption cross section and overestimates the scattering by approximately 14% and 50%, respectively, and the extinction cross section is only 6% smaller than the MSTM results. However, the RDG 2 gives much smaller cross sections for this case. The results of aggregates with monomer size distribution given by $d_{\text{geo}} = 45.5$ nm and $\sigma = 1.13$ are also listed in the table. For this case, the monomers have larger diameters,

TABLE 2
Comparison between the radiative properties of aggregates with different-sized given by the MSTM and the two RDG approximations

Monomer size distribution	Method	C_{ext}	C_{sca}	C_{abs}	g
$d_{geo} = 33$ *nm* and $\sigma = 1.275$	MSTM	0.033	0.0043	0.029	0.57
	RDG 1	0.031	0.0065	0.025	0.56
	RDG 2	0.029	0.0038	0.025	0.56
$d_{geo} = 45.5$ *nm* and $\sigma = 1.13$	MSTM	0.076	0.013	0.063	0.63
	RDG 1	0.067	0.013	0.054	0.60
	RDG 2	0.065	0.012	0.054	0.60

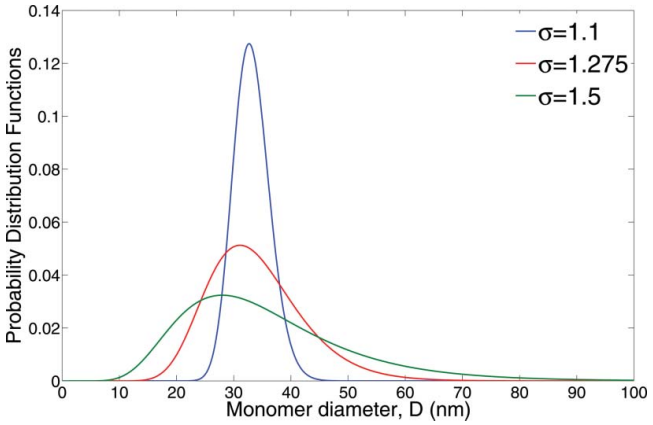

FIG. 4. Lognormal probability distribution of monomer size with geometric mean of 33 nm, and geometric standard deviations of 1.1, 1.275, and 1.5.

whereas the distribution is not as wide as the previous case. Both RDGs obtain the scattering cross sections close to the MSTM results, whereas underestimate the absorption cross sections by approximately 14%. For both cases, the RDG approximation can give asymmetry factors quite close to the exact solutions with relative errors less than 5%. However, considering all radiative properties of the two examples, neither of the two RDG approaches can capture all radiative properties of aggregates with different-sized monomers (besides C_{sca} when the geometric standard deviation is relatively small).

It is obvious that the radiative properties of aggregates with different-sized monomers should be significantly influenced by the monomer size distribution, and the effects of the geometric standard deviation of monomer size distribution are investigated. We fix the geometric mean diameter being 33 nm, and increase the standard deviation from 1.0 to 1.5, i.e., from same-sized monomers to widely distributed ones. Figure 4 shows the probability distribution functions of monomer sizes with geometric mean diameter of 33nm and three geometric standard deviations of 1.1, 1.275, and 1.5. It is clear that as the geometric standard deviation increases the monomer size distribution is significantly widened, with not only more large monomers but also more small ones. When the standard deviation reaches 1.5, the monomer diameters range from 10 nm to over 80 nm. Although the number fraction of large monomers may not increase significantly, e.g., from 4.4% to 15% for monomers with diameters larger than 50nm as σ increases from 1.275 to 1.5, the effects of those larger monomers on the radiative properties are significant.

Figure 5 illustrates the extinction, scattering, and absorption cross sections and single-scattering albedo of aggregates with different-sized monomers as functions of the standard deviation given by the MSTM and the RDGs. The shaded areas indicate the variability (bounded by the average values plus and minus one standard deviation) of the scattering properties given by the MSTM, and 100 aggregate realizations are used for each case. The differences between the MSTM and RDG for the extinction and absorption cross sections exist even for aggregates with same-sized monomers, i.e., $\sigma = 1.0$. Considering that the same-sized monomers are quite small (with size parameter approximately of 0.16), the errors should be introduced by the intra-aggregate multiple scattering effects rather than the non-Rayleigh limitation. As σ increases, the extinction, scattering, and absorption cross sections all increase significantly, because there are more large monomers. The scattering and absorption cross sections at $\sigma = 1.5$ are 2.5 and 1 times larger than the corresponding values at $\sigma = 1.0$, i.e., aggregates with same-sized monomers of $d_{geo} = 33$ nm. The single-scattering albedo also increases from 0.11 to 0.17. Because the RDG approximates the absorption by a simple summation of single monomer absorption, it significantly underestimates the absorption of aggregates. The RDG 1 significantly overestimates the scattering cross sections as σ becomes larger than 1.2, because the Rayleigh approximation is no longer suitable for large monomers, i.e., Equations (8) and (10) break down. To be more specific, the Rayleigh approximation overpredicts the scattering when particle becomes large. However, the RDG 2 seems to give a close approximation for the scattering cross sections of aggregates under different σ values. Because the extinction is the sum of scattering and absorption, it is not difficult to understand the differences between the MSTM and RDG extinction cross sections. Figure 5 illustrates that neither modified RDG approaches can correctly approximate the radiative properties of aggregates with different-sized monomers, especially as the standard deviation of monomer diameters becomes large. It should be noticed that σ values from approximately 1.4 to 1.6 were observed from different fuel combustions (Chakrabarty et al. 2006), and the monomer size distribution should definitely be considered.

Previous studies (Kolokolova et al. 2006; Liu and Mishchenko 2007; Liu and Smallwood 2010b) show that radiative properties averaged over less than 20 aggregate realizations with same-sized monomers are sufficient to give

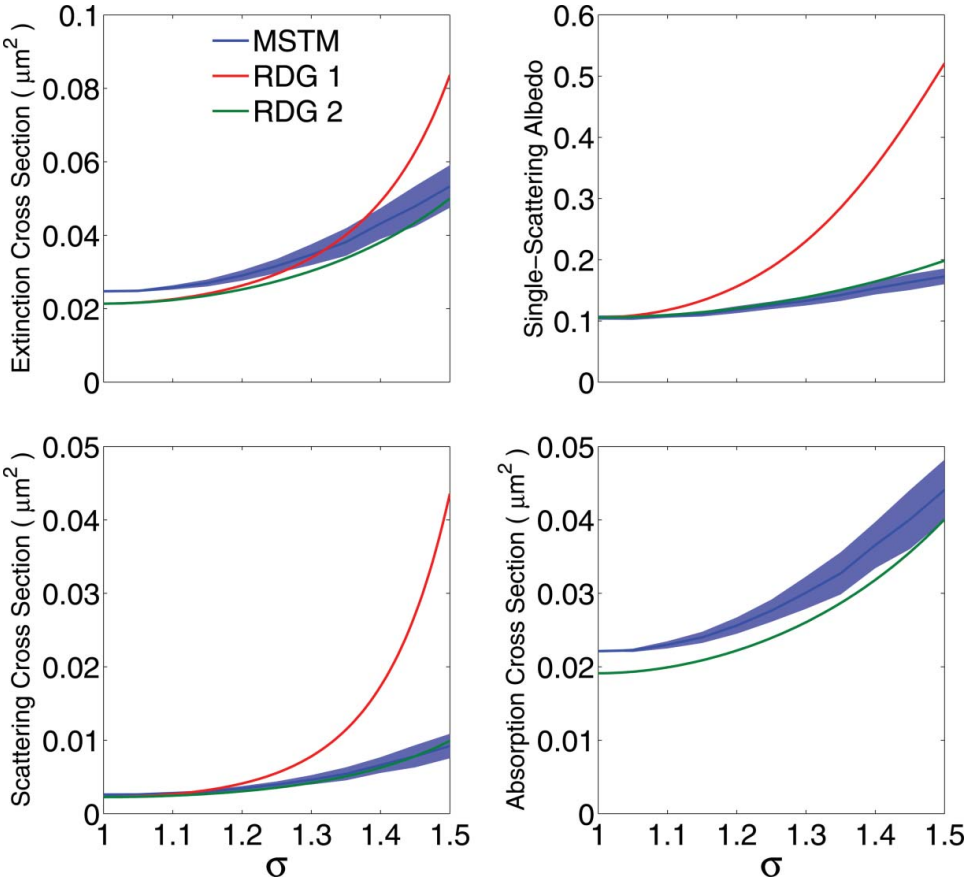

FIG. 5. The integral scattering properties of aggregates with different-sized monomers as functions of geometric standard deviations of monomer size distributions given by the MSTM and the RDGs (two algorithms). The shaded areas depict the averaged values minus and plus one standard deviation for the aggregates with different-sized monomers.

the ensemble-averaged properties of given aggregate parameters. Because the monomer size distribution adds a new freedom to BC particles and their radiative properties, much more aggregate realizations should be considered to obtain accurate ensemble-averaged radiative properties of aggregates with different-sized monomers accurately. Considering the influence of monomer size distribution on aggregate radiative properties, we need to figure out the number of aggregates that should be simulated and averaged to give the ensemble-averaged properties of aggregates with certain fractal parameters and monomer size distributions. Figure 6 gives the averaged extinction, scattering, and absorption cross sections and asymmetry factors as functions of the number of aggregates averaged. Four different aggregate sizes with $N = 100$, 200, 300, and 400 are calculated, and, again, $d_{geo} = 33$ nm and $\sigma = 1.275$ are used. The cross sections are illustrated as the normalized values to that of a single monomer, i.e., C_{ext}/N, C_{sca}/N, and C_{abs}/N in the figure. From the overall trends of the curves, we notice that the average values of the four quantities all become stable when properties of 60 aggregates are averaged. This indicates that radiative properties of 60 aggregate realizations should be safe to represent the ensemble-averaged properties of given parameters for aggregates with different-sized monomers. We expect this number to be significantly affected by the geometric standard deviation of the monomer size distribution, as the monomer size distribution is the main factor that leads the large variances of the radiative properties. The normalized cross sections in the figure represent the average values of each single monomer. Figure 6 indicates that C_{sca}/N increases as N becomes larger, and this is also noticed by Liu et al. (2013). C_{abs}/N is almost a constant for different N values, whereas slightly decreasing trends are obtained by Liu and Smallwood (2010a) and Yon et al. (2008, 2014). The small increases of C_{ext}/N are contributed by the increases in the scattering cross sections. However, only four aggregate sizes are tested in this study, so the trends of the radiative properties obtained here can not be generalized.

The asymmetry factors of the aggregates with different-sized and same-sized monomers show quite close agreement, and similar agreement can be expected for their angular-dependent phase matrix elements. In Figure 7, we compare the normalized phase functions (P_{11}), as well as the ratios of the non-zero phase matrix elements to the phase functions (i.e., P_{22}/P_{11}, P_{33}/P_{11}, P_{44}/P_{11}, P_{12}/P_{11}, and P_{34}/P_{11}), of aggregates with different-sized and same-sized monomers. The aggregate contains 200 monomers,

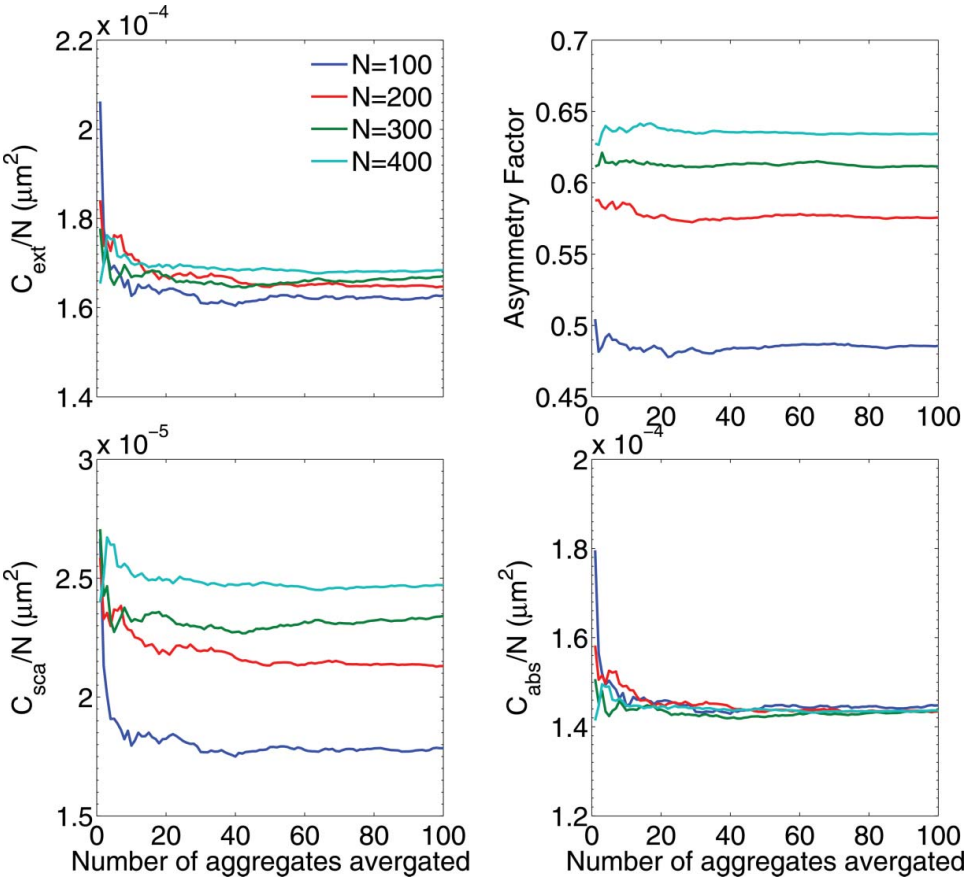

FIG. 6. The averaged scattering properties of aggregates with different-sized monomers as functions of number of aggregates averaged. The exaction, scattering, and absorption cross sections are normalized based on the number of monomers in the aggregates.

and the same monomer size distribution is used. The results for aggregates with different-sized monomers and same-sized monomers with $d_{geo} = 33$ nm and $d_{vol} = 36$ nm are given by the MSTM, and the RDG results are also given in the figure. The results for aggregates with different-sized monomers are averaged over 500 aggregates, whereas single radiative properties of only 50 aggregates are averaged for those with same-sized monomers. In Figure 7, we also illustrate the variability (average values plus or minus one standard deviation are shown in the figure by the shaded areas) of the phase matrix elements of the aggregates with different-sized monomers. The relative differences in the phase function are approximately 12% for the forward scattering and over 15% for the backward scattering, which are similar to those of aggregates with same-sized ones given by Liu and Mishchenko (2007). For the comparison among aggregates with different-sized and same-sized monomers, the phase function given by aggregates of same-sized monomers with $d_{geo} = 33$ nm is close to that of aggregates with different-sized monomers, whereas, as the diameter of same-sized monomer increases to $d_{vol} = 36$ nm, it shows larger forward scattering and smaller backward scattering. Little difference is obtained for P_{12}, P_{22}, P_{33}, and P_{44}, whereas the differences are noticeable for P_{34}/P_{11}. Considering all non-zero elements, the phase matrix elements given by the aggregates with same-sized monomer can provide a rough approximation for those of the different-sized ones, and that with diameter of the geometric mean (d_{geo}) performs better. However, it should be reminded that the integral radiative properties of aggregates with same-sized monomers of d_{vol} are closer to those with different-sized monomers. The results based on the RDG approximation is also listed in the figure, and it shows quite accurate agreement with the exact solution.

From all those results and discussions, we obtain a basic view on the ensemble-averaged radiative properties of aggregates with different-sized monomers. Significant differences are noticed for the amplitude and distribution of the cross sections of aggregates with different-sized monomers, and it is shown that monomer size distribution has to be considered if we want to have a more accurate understanding and parameterization of BC radiative properties.

4. SUMMARY

In this study, we systematically investigate the radiative properties of realistic soot aggregates with different-sized monomers, and compare them with those given by the

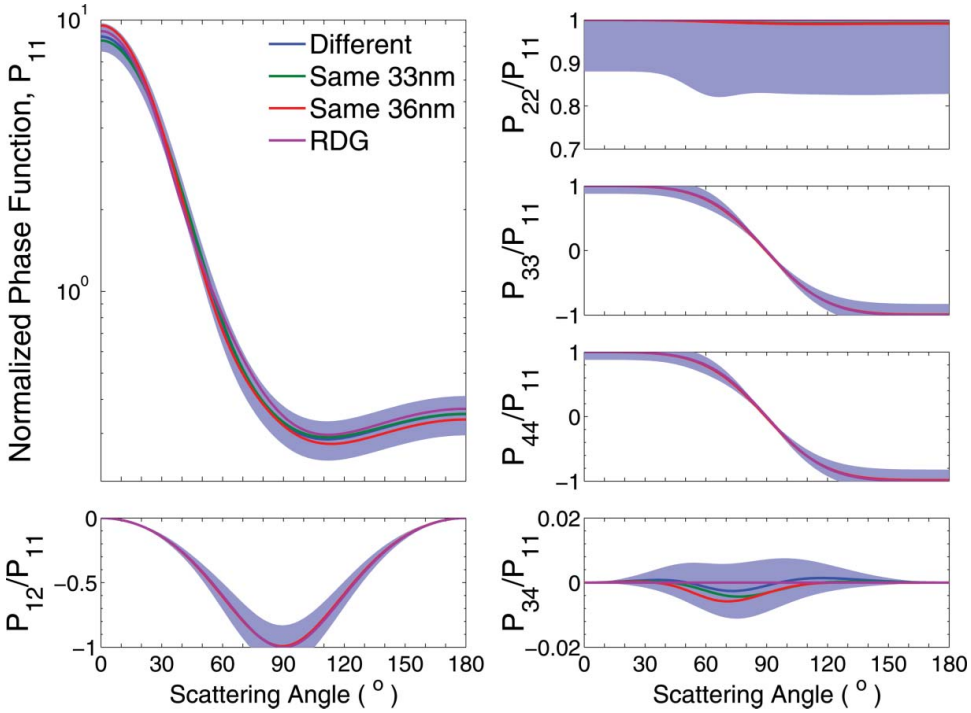

FIG. 7. The normalized phase functions and other non-zero phase matrix elements for the ensemble-averaged aggregates with different-sized and same-sized monomers as functions of scattering angle given by the MSTM and the RDG. The shaded areas depict the averaged values minus and plus one standard deviation for the aggregates with different-sized monomers.

aggregates with same-sized monomers. The present results indicate clear differences between the radiative properties of soot aggregates with different-sized and same-sized monomers: much wider distribution for the radiative properties and much stronger scattering cross sections, whereas the differences on the phase matrix elements are not significant. Our results show that radiative properties given by 60 realizations of aggregates with different-sized monomers should be considered and averaged to give the ensemble-averaged properties of them. The aggregates of same-sized monomers with diameters giving equivalent volume can provide relatively accurate approximations on the extinction and absorption cross sections of aggregates with different-sized monomers, but still underestimates the scattering cross sections by approximately 10%. We also find that the RDG approximations can't give accurate optical quantities for aggregates with different-sized monomers, and this may be due to the neglect of monomer absorptions of intra-aggregate multiple scattering light and the large monomers out of Rayleigh limits.

ACKNOWLEDGMENTS

We thank Dr. Mackowski for his MSTM code. We are grateful for helpful comments made by the two anonymous reviewers.

FUNDING

Chao Liu's research was supported by the Natural Science Foundation of China (NSFC) (Grant No. 41505018), the Natural Science Foundation of Jiangsu Province, China (Grant No. BK20150899) and the Startup Foundation for Introducing Talent of NUIST (Grant No. 2014r067). Fangchao Hu's research was supported by the Natural Science Foundation of China (Grant No. 40975019). Christopher M. Sorensen's research was supported by NSF Directorate for Geosciences AGM 1261651.

REFERENCES

Alexander, D. T., Crozier, P. A. L., and Anderson, J. R. (2008). Brown Carbon Spheres in East Asian Outflow and Their Optical Properties. *Science*, 321:833–836.

Berg, M. J., and Sorensen, C. M. (2013). Internal Fields of Soot Fractal Aggregates. *J. Opt. Soc. Am. A*, 30:1947–1955.

Bescond, A., Yon, J., Ouf, F. X., Ferry, D., Delhaye, D., Gaffié, D., Coppalle, A., and Rozé, C. (2014). Automated Determination of Aggregate Primary Particle Size Distribution by TEM Image Analysis: Application to Soot. *Aerosol Sci. Tech.*, 48:831–841.

Cai, J., Lu, N., and Sorensen, C. M. (1993). Comparison of Size and Morphology of Soot Aggregates as Determined by Light Scattering and Electron Microscope Analysis. *Langmuir*, 9:2861–2867.

Chakrabarty, R. K., Moosmüller, H., Garro, M. A., Arnott, W. P., Walter, J., Susott, R. A., Babbitt, R. E., Wold, C. E., Lincoln, E. N., and Hao, W. M. (2006). Eissions from the Laboratory Combustion of Wildland Fuels:

Particle Morphology and Size. *J. Geophys. Res.*, 111:D07204, doi: 10.1029/2005JD006659.

Chakrabarty, R. K., Moosmüller, H., Arnott, W. P., Garro, M. A., Slowik, J. G., Cross, E. S., Han, J. H., Davidovits, P., Onasch, T. B., and Worsnop, D. R. (2007). Light Scattering and Absorption by Fractal-Like Carbonaceous Chain Aggregates: Comparison of Theories and Experiment. *Appl. Optics*, 46:6990–7006.

Charalampopoulos, T. T. (1992). Morphology and Dynamics of Agglomerated Particulates in Combustion Systems Using Light-Scattering Techniques. *Prog. Energ. Combust.*, 18:13–45.

Charalampopoulos, T. T., and Shu, G. (2002). Effects of Polydispersity of Chainlike Aggregates on Light Scattering Properties and Data Inversion. *Appl. Optics*, 41:723–733.

d' Almeida, G. A., Keopke, P., and Settle, E. P. (1991). *Atmospheric Aerosols: Global Climatology and Radiative Transfer*. A. Deepak, Hampton, VA.

Dankers, S., and Leipertz, A. (2004). Determination of Primary Particle Size Distributions from Time-Resolved Laser-Induced Incandescence Measurements. *Appl. Optics*, 43:3726–3731.

Dobbins, R. A., Fletcher, R. A., and Chang, H. C. (1998). The Evolution of Soot Precursor Particles in a Diffusion Flame. *Combust. Flame*, 115: 285–298.

Dukhin, A. S., Fluck, D., Goetz, P. J., Shilov, V. N., and Dukhin, S. S. (2007). Characterization of Fractal Particles Using Acoustics, Electroacoustics, Light Scattering, Image Analysis, and Conductivity. *Langmuir*, 23: 5338–5351.

Eggersdorfer, M. L., and Pratsinis, S. E. (2012). The Structure of Agglomerates Consisting of Polydisperse Particles. *Aerosol Sci. Tech.*, 46:347–353.

Farias, T. L., Köylü, ü. Ö., and Carvalho, M. G. (1996a). Effects of Polydispersity of Aggregates and Primary Particles on Radiative Properties of Simulated Soot. *J. Quant. Spectrosc. Radiat. Transfer*, 55:357–371.

Farias, T. L., Köylü, ü. Ö., and Carvalho, M. G. (1996b). Range of Validity of the Rayleigh-Debye-Gans Theory for Optics of Fractal Aggregates. *Appl. Optics*, 35:6560–6567.

Filippov, A. V., Zurita, M., and Rosner, D. E. (2000). Fractal-Like Aggregates: Relation between Morphology and Physical Properties. *J. Colloid. Interf. Sci.*, 229:261–273.

Forrest, S. R., and Witten, T. A. (1979). Long-Range Correlations in Smoke Particle Aggregates. *J. Phys. A.-Math. Theor.*, 24:L109.

Helas, G., Gwaze, P., Schmid, O., Annegarn, H. J., Andreae, M. O., and Huth, J. (2006). Comparison of Three Methods of Fractal Analysis Applied to Soot Aggregates from Wood Combustion. *J. Aerosol Sci.*, 37:820–838.

Kolokolova, L., Kimura, H., Ziegler, K., and Mann, I. (2006). Lighter-Scattering Properties of Random-Oriented Aggregates: Do They Represent the Properties of an Ensemble Aggregates? *J. Quant. Spectrosc. Radiat. Transfer*, 100:199–206.

Köylü, ü. Ö., and Faeth, G. M. (1992). Structure of Overfire Soot in Buoyant Turbulent-Diffusion Flames at Long Residence Times. *Combust. Flame*, 89:140–156.

Köylü, ü. Ö., and Faeth, G. M. (1994). Optical Properties of Soot in Buoyant Laminar Diffusion Flames. *J. Heat Trans.*, 116:971–979.

Lehre, T., Jungfleisch, B., Suntz, R., and Bockhorn, H. (2003). Size Distributions of Nanoscaled Particles and Gas Temperatures from Time-Resolved Laser-Induced-Incandescence Measurements. *Appl. Optics*, 42: 2021–2030.

Li, H., Liu, C., Bi, L., Yang, P., and Kattawar, G. W. (2010). Numerical Accuracy of "Equivalent" Spherical Approximations for Computing Ensemble-Averaged Scattering Properties of Fractal Soot Aggregates. *J. Quant. Spectrosc. Radiat. Transfer*, 111:2127–2132.

Liu, Q. H. (1997). The PSTD Algorithm: A Time-Domain Method Requiring Only Two Cells Per Wavelength. *Microw. Opt. Technol. Lett.*, 15:158–165.

Liu, C., Panetta, R. L., and Yang, P. (2012a). Application of the Pseudo-Spectral Time Domain Method to Compute Particle Single-Scattering Properties for Size Parameters up to 200. *J. Quant. Spectrosc. Radiat. Transfer*, 113:1728–1740.

Liu, C., Panetta, R. L., and Yang, P. (2012b). The Influence of Water Coating on the Optical Scattering Properties of Fractal Soot Aggregates. *Aerosol Sci. Tech.*, 46:31–43.

Liu, F., Stagg, B. J., Snelling, D. R., and Smallwood, G. J. (2006). Effects of Primary Soot Particle Size Distribution on the Temperature of Soot Particles Heated by a Nanosecond Pulsed Laser in an Atmospheric Laminar Diffusion Flame. *Int. J. Heat Mass Transfer*, 49:777–788.

Liu, F., and Smallwood, G. J. (2010a). Effect of Aggregation on the Absorption Cross-Section of Fractal Soot Aggregates and Its Impact on LII Modelling. *J. Quant. Spectrosc. Radiat. Transfer*, 111:302–308.

Liu, F., and Smallwood, G. J. (2010b). Radiative Properties of Numerically Generated Fractal Soot Aggregates: The Importance of Configuration Averaging. *J. Heat Trans.*, 132:023308–023308-6.

Liu, F. S., and Smallwood, G. J. (2011). The Effect of Particle Aggregation on the Absorption and Emission Properties of Mono- and Poly-Disperse Soot Aggregates. *Appl. Phys. B*, 104:343–355.

Liu, F., Wong, C., Snelling, D. R., and Smallwood, G. J. (2013). Investigation of Absorption and Scattering Properties of Soot Aggregates of Different Fractal Dimension at 532 nm Using RDG and GMM. *Aerosol Sci. Tech.*, 47:1393–1405.

Liu, L., and Mishchenko, M. I. (2005). Effects of Aggregation on Scattering and Radiative Properties of Soot Aerosols. *J. Geophys. Res.*, 110: doi:10.1029/2004JD005649.

Liu, L., and Mishchenko, M. I. (2007). Scattering and Radiative Properties of Complex Soot and Soot-Containing Aggregate Particles. *J. Quant. Spectrosc. Radiat. Transfer*, 106:262–273.

Mackowski, D. W. (1994). Calculation of Total Cross Sections of Multiple Sphere Cluster. *J. Opt. Soc. Am. A*, 11:2851–2861.

Mackowski, D. W., and Mishchenko, M. I. (1996). Calculation of the T-Matrix and the Scattering Matrix for Ensembles of Spheres. *J. Opt. Soc. Am. A*, 13:2266–2278.

Martin, J. E., and Hurd, A. J. (1987). Scattering from Fractals. *J. Appl. Crystallogr.*, 20:61–78.

Menon, S., Hansen, J., Nazarenko, L., and Luo, Y. (2002). Climate Effects of Black Carbon Aerosols in China and India. *Science*, 297:2250–2253.

Moffet, R. C., and Prather, K. A. (2009). In-Situ Measurements of the Mixing State and Optical Properties of Soot with Implications for Radiative Forcing Estimates. *P. Natl. Acad. Sci.*, 106:11872–11877.

Purcell, E. M., and Pennypacker, C. R. (1973). Scattering and Absorption of Light by Nonspherical Dielectric Grains. *Astrophys. J.*, 186:705–714.

Ramanathan, V., and Carmichael, G. (2008). Global and Regional Climate Change Due to Black Carbon. *Nature Geoscience*, 1:221–227.

Sorensen, C. M., Cai, J., and Lu, N. (1992). Test of Static Structure Factors for Describing Light Scattering from Fractal Soot Aggregates. *Langmuir*, 8:2064–2069.

Sorensen, C. M., and Roberts, G. C. (1997). The Prefactor of Fractal Aggregates. *J. Colloid. Interf. Sci.*, 186:447–452.

Sorensen, C. M. (2001). Light Scattering by Fractal Aggregates: A Review. *Aerosol Sci. Tech.*, 35:648–687.

Skorupski, K., and Mroczka, J. (2014). Effect of the Necking Phenomenon on the Optical Properties of Soot Particles. *J. Quant. Spectrosc. Radiat. Transfer*, 141:40–48.

Tian, K., Liu, F., Thomson, K. A., Snelling, D. R., Smallwood, G. J., and Wang, D. S. (2004). Distribution of the Number of Primary Particles of Soot Aggregates in a Nonpremixed Laminar Flame. *Combust. Flame*, 138:195–198.

van de Hulst, H. C. (1957). *Light Scattering by Small Particles*, Dover, New York.

Van-Hulle, P., Weill, M. E., Talbaut, M., and Coppalle, A. (2002). Comparison of Numerical Studies Characterizing Optical Properties of Soot Aggregates for Improved EXSCA Measurements. *Part. Part. Syst. Char.*, 19:47–57.

Xu, Y. L. (1995). Electromagnetic Scattering by an Aggregate of Spheres. *Appl. Optics*, 34:4573–4588.

Xu, Y. L., and Gustafson, B. Å. S. (2001). A Generalized Multiparticle Mie-Solution: Further Experimental Verification. *J. Quant. Spectrosc. Radiat. Transfer*, 70:395–419.

Yang, P., and Liou, K. N. (1996). Finite-Difference Time Domain Method for Light Scattering by Small Ice Crystals in Three-Dimensional Space. *J. Opt. Soc. Am. A*, 13:2072–2085.

Yee, K. S. (1966). Numerical Solution of Initial Boundary Value Problems Involving Maxwell's Equations in Isotropic Media. *IEEE Trans. Antennas Propagat.*, 14, 302–307.

Yin, J. Y., and Liu, L. H. (2010). Influence of Complex Component and Particle Polydispersity on Radiative Properties of Soot Aggregate in Atmosphere. *J. Quant. Spectrosc. Radiat. Transfer*, 111:2115–2126.

Yon, J., Roze, C., Girasole, T., Coppalle, A., and Mees, L. (2008). Extension of RDG-FA for Scattering Prediction of Aggregates of Soot Taking into Account Interactions of Large Monomers. *Part. Part. Syst. Char.*, 25: 54–67.

Yon, J., Liu, F., Bescond, A., Caumont-Prim, C., Rozé, C., Ouf, F., and Coppalle, A. (2014). Effects of Multiple Scattering on Radiative Properties of Soot Fractal Aggregates. *J. Quant. Spectrosc. Radiat. Transfer*, 133: 374–381.

Yon, J., Bescond, A., and Liu, F. (2015). On the Radiative Properties of Soot Aggregates Part 1: Necking and Overlapping. *J. Quant. Spectrosc. Radiat. Transfer*, 162:197–206.

Yurkin, M. A., and Hoekstra, A. G. (2011). The Discrete Dipole Approximation Code ADDA: Capabilities and Known Limitations. *J. Quant. Spectrosc. Radiat. Transfer*, 112:2234–2247.